A linear-quadratic-Gaussian approach for automatic flight control of fixed-wing unmanned air vehicles

C.-S. Lee
p4897702@mail.ncku.edu.tw
W.-L. Chan, S.-S. Jan and F.-B. Hsiao
Institute of Aeronautics and Astronautics
National Cheng Kung University
Taiwan

ABSTRACT

This paper presents the design and implementation of automatic flight controllers for a fixed-wing unmanned air vehicle (UAV) by using a linear-quadratic-Gaussian (LQG) control approach. The LQG design is able to retain the guaranteed closed-loop stability of the linear-quadratic regulator (LQR) while having incomplete state measurement. Instead of feeding back the actual states to form the control law, the estimated states provided by a separately designed optimal observer, i.e. the Kalman filter are used. The automatic flight controllers that include outer-loop controls are constructed based on two independent LQG regulators which govern the longitudinal and lateral dynamics of the UAV respectively. The resulting controllers are structurally simple and thus efficient enough to be easily realized with limited onboard computing resource. In this paper, the design of the LQG controllers is described while the navigation and guidance algorithm based on Global Positioning System (GPS) data is also outlined. In order to validate the performance of the automatic flight control system, a series of flight tests have been conducted. Significant results are presented and discussed in detail. Overall, the flight-test results show that it is highly feasible and effective to apply the computationally efficient LQG controllers on a fixed-wing UAV system with a relatively simple onboard system. On the other hand, a fully automatic 44km cross-sea flight demonstration was successfully conducted using the LQG-based flight controllers. Detailed description regarding the event and some significant flight data are given.

NOMENCLATURE

$\mathbf{A},\mathbf{B},\mathbf{C},\mathbf{H}$	state-space system matrices
d	perpendicular distance between aircraft and desired flight path
h	altitude
h_{ref}	reference altitude
J	cost function
$\mathbf{K}$	optimal feedback gain in linear-quadratic regulator (LQR)
k	discrete system time step
$\mathbf{L}$	optimal estimator gain in Kalman filter
$\mathbf{P}$	solution of discrete algebraic Ricatti equation
m	variable in straight-line-following guidance law
p,q,r	components of angular velocity vector in body axes
$\mathbf{Q},\mathbf{R}$	LQR weighting function
R_{WP}	waypoint 'pass-through' criterion
s	distance between aircraft and target waypoint
$\mathbf{u}$	input vector
V	total airspeed
$\mathbf{v}$	measurement noise vector
$\mathbf{w}$	process noise vector
$\mathbf{x}$	system state vector
$\hat{\mathbf{x}}$	predicted state sequence or Kalman state sequence
$\mathbf{y}$	output state vector
α	angle-of-attack
β	angle-of-sideslip

Paper No. 3563. Manuscript received 12 April 2010, revised version received 3 October 2010, accepted 26 October 2010.

Δ	perturbation from trim value
$\delta_e,\delta_a,\delta_r$	deflection angle of elevator, aileron, rudder
$\phi\theta\Psi$	Euler angles (bank, pitch, yaw)
σ	bearing from previous to next waypoint

ABBREVIATIONS

AHRS	attitude and heading reference system
COM port	communication port
GCS	ground control station
GPS	Global Positioning System
ISTAR	intelligence, surveillance, target acquisition, and reconnaissance
LQG	linear-quadratic-Gaussian
LQR	linear-quadratic regulator
MIMO	multi-input multi-output
NED	north-east-down
OBC	onboard computer
PEM	prediction error method
PID	proportional-integral-derivative
PWM	pulse-width modulation
RMRL	remotely piloted vehicle and microsatellite research laboratory
RPM	revolution per minute
SIB	sensor integration board
SMB	servo management board
UAV	unmanned air vehicle
WP	waypoint

1.0 INTRODUCTION

To say that the unmanned air vehicles (UAVs) are gaining popularity is a huge understatement. As more countries around the world begin to acknowledge and actively pursue UAV systems to augment their own intelligence, surveillance, target acquisition and reconnaissance (ISTAR) capabilities, the research and development of UAV-related technologies have received unprecedented attention and interest over recent years. Interestingly, majority of the UAV systems that are in service nowadays have fixed wing configuration. Fixed-wing UAVs, especially the larger ones with gross weight in excess of 100kg, own distinct advantages over other configurations in terms of payload capacity, operational speed, altitude, range and endurance. This is supported by the fact that most of the world's renowned UAVs such as the Global Hawk, Predator, Shadow, Heron, etc are all fixed-wing aircraft. In conjunction with that, this paper therefore focuses on the automatic control strategies developed exclusive of conventional fixed-wing UAV systems.

In a manned aircraft, the onboard human pilot plays a crucial part in the closed-loop control system by taking visual data in addition to the sensor measurements and then reacts accordingly. For an UAV however, the automatic flight control system needs to cope with the absence of the human pilot in the loop. One of the biggest challenges is to obtain a sufficiently accurate system model which describes the aircraft dynamics and its interaction with the operating environment. Adding to the difficulty is the fact that an aircraft typically subject to unpredictable atmospheric environmental disturbances such as crosswind, gust, wind shear, turbulence, and so on. Moreover, for the relatively small UAVs (less than 30kg), control system designers are faced with penalties in terms of size, weight and cost. This means that limited sensors which provide system states and situational awareness are available onboard an UAV. To deal with that inadequacy, designers often turn to automatic control strategies that can handle significant modeling and environmental uncertainties with minimal sensor measurements. One of the most popular control methods is the proportional-integral-derivative (PID) controller. In fact, it has been successfully implemented on small UAV systems as reported by Erdos and Watkins[1], Beard *et al*[2] and Hsiao *et al*[3]. However, more than often the gain tuning process relies on trial-and-error and a priori knowledge of the system to achieve the best possible control performance. In some cases, a bad choice of gains may lead to system instability which is potentially catastrophic for an UAV.

Thanks to the remarkable advancement in the computing power, flight control designers have been able to explore the feasibility of implementing more advanced and complex control strategies on UAVs. Although based on linearised models, flight controllers developed under the framework of optimal control have been applied to UAV systems with encouraging results. Compared with other advanced control theories such as nonlinear control and robust control, the optimal control yields simpler controller while still able to retain some degree of guaranteed robustness over system uncertainties. Moreover, it is applicable to multi-input multi-output (MIMO) system under the time-domain architecture. These features make the linear-quadratic based control synthesis, in particular the linear-quadratic regulator (LQR) highly suitable for the automatic flight control of UAVs. For instance, Montgomery[4] and Cho *et al*[5] have successfully implemented the LQR flight controllers on their respective UAV systems. Another example can be found in the work of Tuzcu *et al*[6] on the stability and control of a high-altitude, long-endurance UAV. The LQR is attractive in the sense that the control theory is well-established mathematically and the resulting control law is simple and elegant. Plus, the optimal control gains are automatically generated in the solution of the control equations. This means that in its core, the LQR algorithm is an automated way of finding an appropriate state-feedback controller. Its biggest pitfall, however, is the requirement of the real-time full-state measurement which is often unavailable in practice[7]. In conjunction with that, the linear-quadratic-Gaussian (LQG) controller is an extension of the LQR where the unmeasured states are estimated using an optimal observer, i.e. the Kalman filter. This gives the LQG the advantage of dealing with the uncertain linear systems disturbed by the additive white Gaussian noise while having incomplete system state information available for the control-loop feedback. The feature makes it ideal to serve as an automatic flight controller for UAVs. In fact, Lee *et al*[7] have shown that the LQG works very well as the baseline stability augmentation autopilot for a 30kg fixed-wing UAV which handles the inner-loop control of the system.

In light of the above discussions, this paper attempts to demonstrate the feasibility of realizing the automatic flight controllers for the Spoonbill UAV by adopting the LQG design methodology and further extend the controllers to include the outer-loop control. The Spoonbill UAV[7,8] is an experimental research platform under development by the Remotely Piloted Vehicle and Microsatellite Research Laboratory (RMRL) of National Cheng Kung University, Taiwan. The UAV system was built under the context of Spoonbill project where the UAV is supposed to perform an automatic cross-sea demonstration flight over a distance of approximately 44km by August 2009. The background of the Spoonbill project and the cross-sea flight demonstration are given in Lee *et al*[7]. In practice, two independent linear controllers are used to govern the longitudinal and lateral/directional dynamics of the aircraft respectively. Considerable efforts have been made on the aircraft modeling process as well where two linear models describing the aircraft's longitudinal and lateral dynamic behaviours are obtained via a system identification approach. Essentially, actual input-output data of the aircraft system collected through flight tests are used to determine the unknown system parameters using a system identification technique. In particular, a combination of subspace and prediction-error method identification algorithms was used[9,10]. The resulting models are expressed in the form of a state-space representation which is compulsory in the synthesis of LQG controllers.

The remaining parts of this paper are organised as follows: First, the overall system configuration of the Spoonbill UAV system is briefly introduced in Section 2. In particular, the air vehicle, onboard

https://doi.org/10.1017/S0001924000005340 Published online by Cambridge University Press

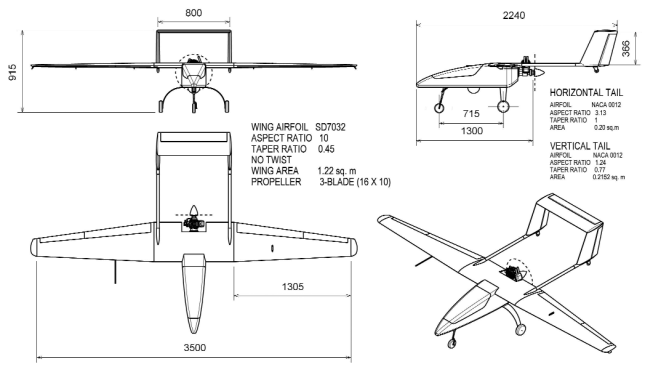

Figure 1. Schematic drawings showing general layout and dimensions of SP-80.

Figure 2. SP-80 resting on a deserted salt field.

system, ground control system and payload system are described. Then, the next section provides the synthesis of the automatic flight control system based on the LQG technique. The same section also details the navigation and guidance algorithm adopted in the UAV system which is based on the Global Positioning System (GPS) data. Subsequently, significant flight-test results, which represent different phases of the validation of the automatic flight controllers, are presented and discussed. Finally, further details regarding the cross-sea flight demonstration are covered in Section 5 before some concluding remarks wrap up the paper in Section 6.

2.0 SYSTEM CONFIGURATION

The air vehicle of the Spoonbill UAV system used in this work is designed by the RMRL and it is designated as SP-80. Figure 1 and Fig. 2 depict the high-wing, twin-boom, pusher engine type layout of the aircraft which has a wingspan of 3·50m (without Hoerner wingtips), an aspect ratio of 10 and an overall length of 2·24m. The aircraft is capable of lifting off with a maximum gross weight of 30kg, powered by an 80cc two-stroke twin-piston engine which runs on gasoline fuel. At the maximum weight configuration, 3kg of gasoline fuel keeps the aircraft aloft for approximately one hour. Typically, the cruising speed is maintained between 90–110km/h which would give the aircraft a maximum range of approximately 100km assuming normal wind condition. The entire airframe is constructed from a mix of composite and wood materials.

Figure 3 shows the fuselage being fully packed with the onboard system which is composed of various subsystems and components.

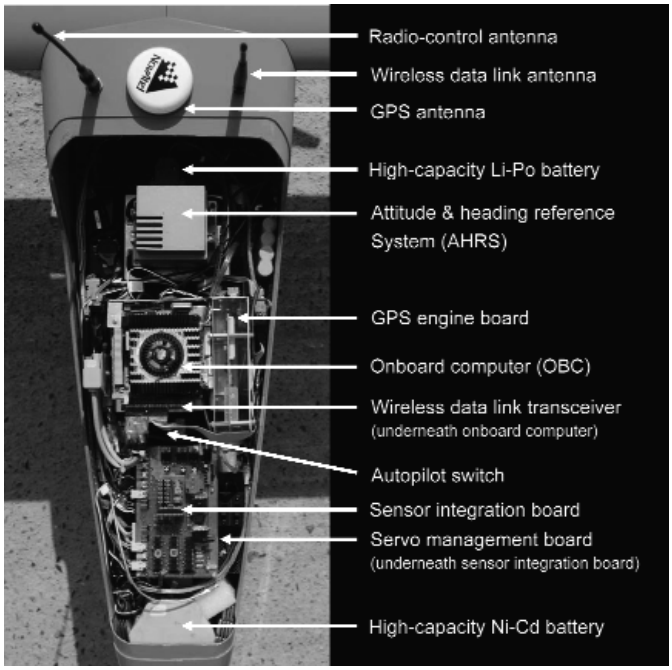

Figure 3. Onboard avionics system.

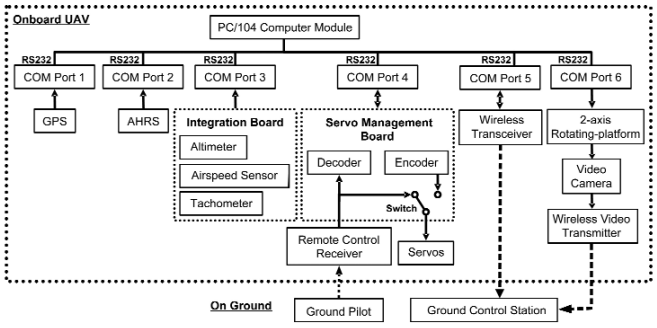

Figure 4. Onboard system architecture of Spoonbill UAV system.

Interestingly, the overall onboard system architecture of Spoonbill UAV is actually quite simple as illustrated in Fig. 4. The core of the onboard system is the onboard computer (OBC) which is a PC/104 computer module that operates under a Windows-based embedded operating system. All peripheral subsystems communicate with the OBC via communication ports (COM ports) that use RS-232 protocol at a rate of 20Hz. The primary task of the OBC is to acquire various sensor data, perform flight-control computation, and record selected flight parameters. All data enter OBC in a digital format which means that they are preprocessed beforehand. This is done by means of microcontrollers, which significantly improve the efficiency and performance of the OBC.

The primary onboard sensors include an attitude and heading reference system (AHRS), a GPS receiver, and a sensor integration board (SIB) which integrates the air data sensors and the engine tachometer. Both the AHRS and GPS receiver are off-the-shelf products and each of them occupies one communication port (COM port) as shown in Fig. 4. The GPS receiver provides global position and velocity data of the aircraft while the AHRS measures the body-frame angular speeds, attitude angles, accelerations, and earth magnetic field. The sensor integration board (SIB) and servo management board (SMB), however, are designed, fabricated and tested by the RMRL. The SIB processes analog signals acquired from the air data sensors (airspeed sensor and altimeter) and

https://doi.org/10.1017/S0001924000005340 Published online by Cambridge University Press

Figure 5. Onboard video camera and zthe wireless video transmission antenna.

tachometer, concatenates them into a single package of binary code and sends them to the OBC. The SMB basically deals with the pulse-width modulation (PWM) signals associated with the servomotors which drive the control surfaces of the aircraft. While decoding the control signals given by the ground pilot during manual flight, the SMB also generates the PWM signals to be fed to the servomotors corresponding to the command inputs calculated by the flight control program during automatic mode. The switch between manual and automatic control of the aircraft is accomplished within the SMB as well (see Fig. 4). Automatic flight of an UAV would not be possible without an effective and reliable SMB.

On the other hand, the operating personnel on the ground can keep constant contact with the airborne system via a wireless communication link. Vital data which reflect the aircraft condition are continuously relayed back to the ground control station (GCS) at a rate of 2Hz. Commands and changes of system parameters can also be uploaded to the onboard system via the same data link. However, the effective range of the wireless data link coupled with a directional antenna is limited to approximately 25km line-of-sight.

In addition to that, another wireless link transmits video images from the onboard camera back to the ground. A miniature gimbaled video camera installed at the belly of the fuselage constitutes the payload of the Spoonbill UAV system (see Fig. 5). The video camera is mounted onto a two-axis rotating-platform which permits the camera to rotate along the pitch and roll axes relative to the aircraft body-frame co-ordinates. Hence, with the knowledge of the attitude of the aircraft (readily measured by AHRS), it is possible for the camera to maintain a desired constant orientation regardless of the dynamic motion of the aircraft itself. For instance, the video camera may be commanded to always point directly towards the ground surface.

3.0 AUTOMATIC FLIGHT CONTROLLERS

3.1 Aircraft dynamics

It is not uncommon to decouple the aircraft dynamics into independent longitudinal and lateral/directional dynamics. This is especially legitimate for conventionally configured (tail-aft) fixed-wing aircraft such as SP-80. Furthermore, Nelson[11] among others, has shown that both longitudinal and lateral dynamics of an aircraft may be expressed in a linear discrete-time state-space representation as the following:

$$\begin{aligned}\mathbf{x}(k+1) &= \mathbf{A}\mathbf{x}(k) + \mathbf{B}\mathbf{u}(k) + \mathbf{H}\mathbf{w}(k)\\ \mathbf{y}(k) &= \mathbf{C}\mathbf{x}(k) + \mathbf{v}(k)\end{aligned} \quad \ldots (1)$$

where k is the sequential number of time-step. Note that **x**, **u**, **y**, **w** and **v** are the system state, control input, measured output, process noise and measurement noise vectors respectively. It is assumed that **w** and **v** are additive white Gaussian noise. The remaining **A**, **B**, **C** and **H** are the so-called system matrices where unknown derivatives pertaining to the aerodynamic forces and moments acting on the aircraft constitute their elements. Essentially, the system matrices determine the dynamics of the aircraft motion and they ought to be time-invariant with respect to a particular equilibrium (trimmed) flight condition. Note that the choice of the states and outputs are not unique. In particular, for the Spoonbill UAV system, the following are defined for the longitudinal model:

$$\begin{aligned}\mathbf{x} &= \left[\Delta V, \Delta\alpha, \Delta q, \Delta\theta, \Delta h\right]^T\\ \mathbf{y} &= \left[\Delta V, \Delta q, \Delta\theta, \Delta h\right]^T\\ \mathbf{u} &= \left[\Delta\delta_e\right]\end{aligned} \quad \ldots (2)$$

where V, α, q, θ, δ_e, are the airspeed, angle-of-attack, pitch rate, pitch angle, altitude and elevator deflection respectively. Similarly, for the lateral model,

$$\begin{aligned}\mathbf{x} &= \left[\Delta\beta, \Delta p, \Delta r, \Delta\phi\right]^T\\ \mathbf{y} &= \left[\Delta p, \Delta r, \Delta\phi\right]^T\\ \mathbf{u} &= \left[\Delta\delta_a, \Delta\delta_r\right]^T\end{aligned} \quad \ldots (3)$$

where β, p , r, ϕ, δ_a, δ_r are the sideslip angle, roll rate, yaw rate, bank angle, aileron deflection, and rudder deflection, respectively. Note that the symbol Δ denotes that all states, **x**, measured outputs, **y**, and inputs, **u** are perturbations from the trimmed conditions (see Lee[10] for complete derivation). Moreover, all vectors are relative to the aircraft's body-frame co-ordinates where the origin coincides with the aircraft center of gravity while sign convention follows the standard typically used in Western aeronautics community.

In order to proceed with the design of the automatic flight controllers, the unknown system matrices, **A**, **B**, **C** and **H** for both longitudinal and lateral models need to be determined, specifically for the Spoonbill UAV. The importance of an accurate aircraft model for the controller design can never be overemphasized. Hence, considerable efforts were made to obtain models that adequately describe the aircraft dynamics. In particular, the authors successfully implemented a combined subspace/PEM (prediction error method) system identification technique to retrieve the unknown system matrices for both longitudinal and lateral models in their previous works[9,10].

3.2 Linear-quadratic-Gaussian regulator

The automatic flight controllers of the Spoonbill UAV system are constructed based on the linear-quadratic-Gaussian (LQG) regulator. One of the appealing characteristics of LQG control approach is that it handles MIMO uncertain linear systems disturbed by the additive white Gaussian noise while having incomplete state information (i.e. not all of the state variables are measured and available for feedback). This makes it ideal to deal with the aircraft system described in previous section. In essence, the LQG regulator is a combination of the linear-quadratic regulator (LQR) and the Kalman filter. For a system expressed in the linear state-space form such as Equation (1), the linear-quadratic control theory assumes a full-state negative feedback control law:

$$\mathbf{u}(k) = -\mathbf{K}\mathbf{x}(k)$$

where the optimal constant feedback gain, K is obtained such that the quadratic cost function, J

https://doi.org/10.1017/S0001924000005340 Published online by Cambridge University Press

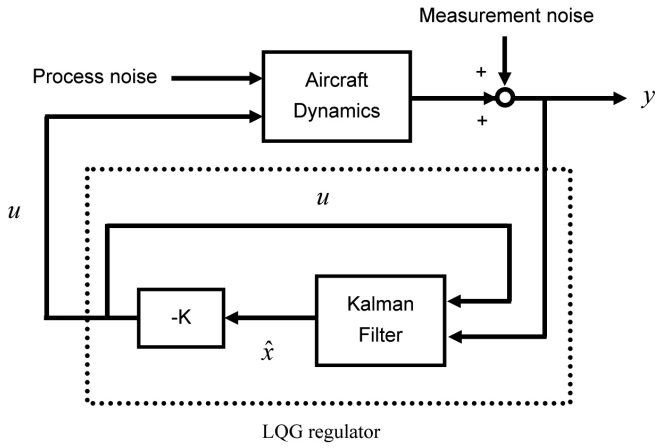

Figure 6. LQG regulator.

$$J = \sum_{k=1}^{\infty} \left[\mathbf{x}(k)^T \mathbf{Q} \mathbf{x}(k) + \mathbf{u}(k)^T \mathbf{R} \mathbf{u}(k) \right]$$

is minimised. Note that **Q** and **R** are the symmetric positive semi-definite weighting matrices which determine the performance of the state regulation and the amount of control effort incurred, respectively. This optimisation problem is well-established and long solved where **K** is readily attainable by solving the so-called discrete algebraic Ricatti equation[12] for **P**:

$$\mathbf{P} = \mathbf{Q} + \mathbf{A}^{\mathrm{T}}\mathbf{P}\mathbf{A} - \left(\mathbf{A}^{\mathrm{T}}\mathbf{P}\mathbf{B}\right)\left(\mathbf{R} + \mathbf{B}^{\mathrm{T}}\mathbf{P}\mathbf{B}\right)^{-1}\left(\mathbf{B}^{\mathrm{T}}\mathbf{P}\mathbf{A}\right)$$

which yields

$$\mathbf{K} = \left(\mathbf{R} + \mathbf{B}^{\mathrm{T}}\mathbf{P}\mathbf{B}\right)^{-1}\left(\mathbf{B}^{\mathrm{T}}\mathbf{P}\mathbf{A}\right)$$

On the other hand, since the Kalman filter is basically an optimal observer (estimator), it can be constructed for the system of Equation (1), under the same framework of the linear-quadratic control problem as the LQR but with its own weighting matrices, optimal observer gain, and corresponding algebraic (filter) Ricatti equation[12].

The full-state-feedback LQR is attractive because the closed-loop system is guaranteed to be stable[13]. In addition, it also has certain guaranteed robustness properties that make it suitable for application on flight controls. However, full-state measurement is rarely available in practice. In fact, this is exactly the case for the Spoonbill UAV system where the angle-of-attack, α and the sideslip angle, β are not measured. A way to circumvent this deficiency is to incorporate an observer, e.g. a Kalman filter into the controller to estimate the system states using the available outputs, y and known control inputs, u. Now, instead of using the actual states, x, the estimated states, is fed back to form the control law:

$$\mathbf{u}(k) = -\mathbf{K}\hat{\mathbf{x}}(k)$$

The concatenation of LQR and Kalman filter forms the LQG regulator shown in Fig. 6. When implemented on an aircraft system, the LQG regulator basically controls the inner-loop system where the aircraft is maintained at the steady-state trimmed conditions where the states, **x** and outputs, **y** are regulated to zero in the presence of disturbances. For the Spoonbill UAV, two independent LQG regulators are designed based on the longitudinal and lateral models separately which govern the corresponding aircraft dynamics. To make the LQG approach more attractive, the separation principle infers that the state feedback gain in LQR, **K** and the observer gain in Kalman filter, **L** may be designed separately

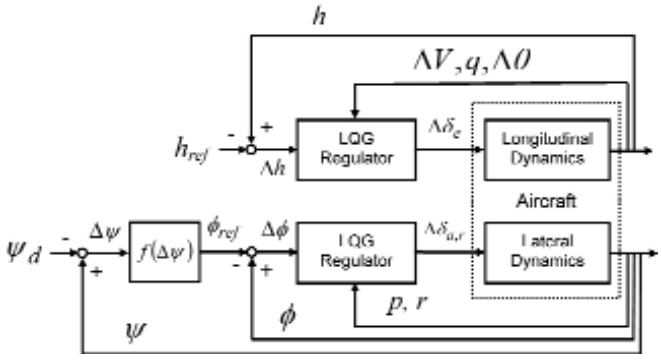

Figure 7. Nonzero-set-point tracking controllers.

to yield desired closed-loop plant and observer behaviors (see Stevens and Lewis[13], pp 561). Among the ramifications of the separation principle are that the closed-loop stability is guaranteed and proven software is available to solve the matrix design equations (respective algebraic Ricatti equations) that yield **K** and **L**. Moreover, the solution is unique and constitutes a linear multi-variable feedback control law that is easily computed and implemented on a digital onboard computer. In practice, the authors use MATLAB® programming package to solve for the control law while the actual discrete controllers are executed in Borland C++ Builder® code on the onboard computer. Consistent with the onboard system's data sampling rate, the control law is running at an update rate of 20Hz. Detailed and complete presentation of the controller synthesis can be found in Lee[10].

3.3 Nonzero-set-point tracking controllers

In their previous work[7], the authors have proven that the LQG regulators work very well as the baseline stability augmentation autopilot for the Spoonbill UAV. It turns out that the LQG regulators are very effective in maintaining the aircraft states and outputs while having good disturbance rejection capability. It is noteworthy that the aircraft typically flies in an environment susceptible to unpredictable crosswinds and sudden gusts, let alone inherent noises embedded in the sensor data. In the present work, the authors further explore the feasibility of extending the LQG regulators into nonzero-set-point tracking controllers.

Recall from Equation (2) and (3) that the aircraft states and outputs are not absolute measurement from flight but perturbations from the steady-state trimmed condition. This is the very fact that made it possible to modify the original LQG regulator into a set-point tracking controller without much additional effort. This is accomplished by simply adjusting the reference values to those of the desired aircraft outputs. Obviously, the further away the reference value is from the actual trimmed value, the poorer the tracking performance of the controller will be. This is because the system dynamics is no longer accurately described by the models which are identified with respect to a certain trimmed condition.

Figure 7 shows the nonzero-set-point tracking controllers built upon the LQG regulators for the Spoonbill UAV. Note that the symbol Δ of variables p, q, and r are dropped since the reference values of the angular rates are always zero at trimmed condition. Also, it is important to realise that the number of outputs that may be perfectly tracked cannot be more than the total number of inputs the system has. For the longitudinal control, there is only one input, i.e. the elevator deflection. Hence only the altitude is selected to be tracked where the difference between the reference altitude, h_{ref} and the measured altitude, h is fed into the LQG regulator. Nevertheless, the present longitudinal controller is not capable of tracking any arbitrary altitudes, especially when the altitude change relative to the

https://doi.org/10.1017/S0001924000005340 Published online by Cambridge University Press

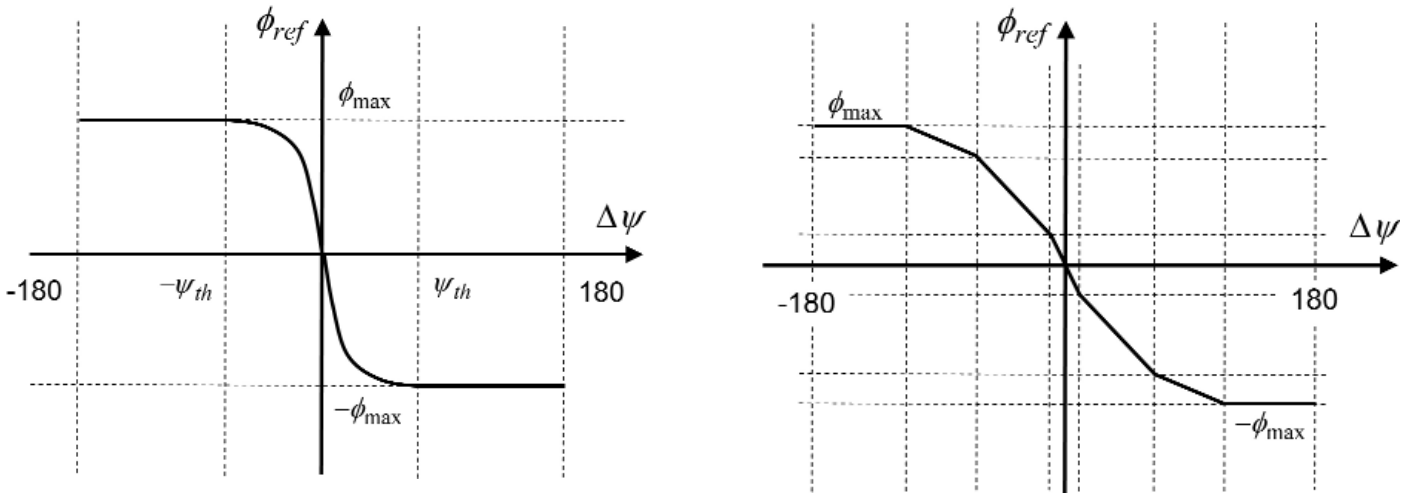

(a) (b)

Figure 8. Heading controllers.

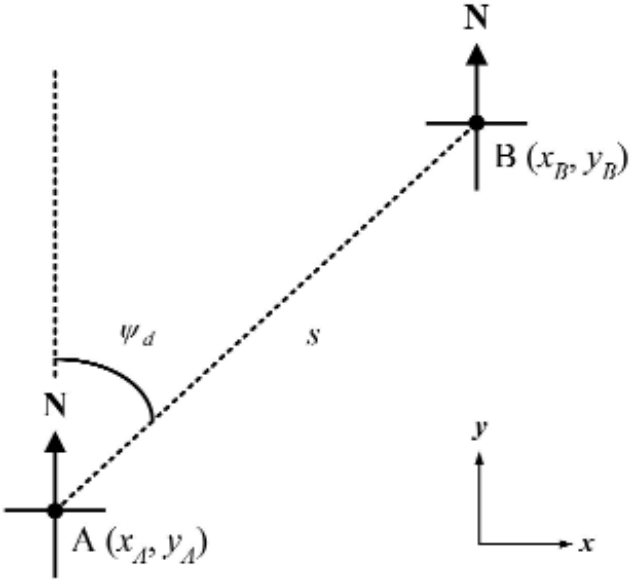

Figure 9. Point-to-point guidance law.

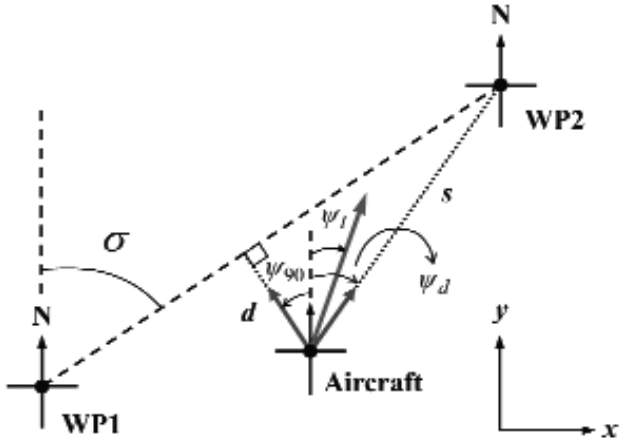

Figure 10. Straight-line-following guidance law.

initial value is somewhat large. This is because when the aircraft is to climb or descent over significant amount of altitude gap, an associated change of engine thrust is usually required. Recall, however, that the longitudinal model as shown in Equation (2) does not include the engine throttle input which dictates the forward thrust of the aircraft. Therefore, the present longitudinal controller works somewhat like an altitude-hold autopilot.

On the other hand, the lateral controller is able to track the arbitrary reference bank angles, ϕ_{ref} by the aileron and rudder deflections. Furthermore, a stable and sustained rolling motion is sufficient to steer the aircraft towards the desired headings, Ψ_d which in turn would determine the flight path of the aircraft. This can be accomplished through a simple controller which relates the difference between the actual and desired heading, $\Delta\Psi$ with ϕ_{ref}. Two examples of such relations are shown in Fig. 8. Note that the arbitrary parameters, Ψ_{th} and ϕ_{max} are determined through actual flight tests.

3.4 Navigation and guidance law

Currently, the navigation of the Spoonbill UAV relies solely on the Global Positioning System (GPS). If the previously described heading controller is capable of tracking arbitrary headings with a satisfactory performance, and with the independent longitudinal controller holding altitude during turning maneuvers, then it is possible for the aircraft to perform waypoint-following automatic flight guided by real-time GPS position data. Since the position data of the aircraft is provided in the geodetic latitude and longitude format, it is necessary to convert them onto a local Cartesian coordinate frame first, for instance the North-East-Down (NED) frame. Then, referring to Fig. 9, a rudimentary point-to-point navigation and guidance law can be derived from the two-dimensional coordinates (x-y) of the aircraft (point A) and the destination waypoint (point B) at each moment. Consequently, the desired heading, Ψ_d and the distance towards the waypoint, s can be easily computed at each control loop via

https://doi.org/10.1017/S0001924000005340 Published online by Cambridge University Press

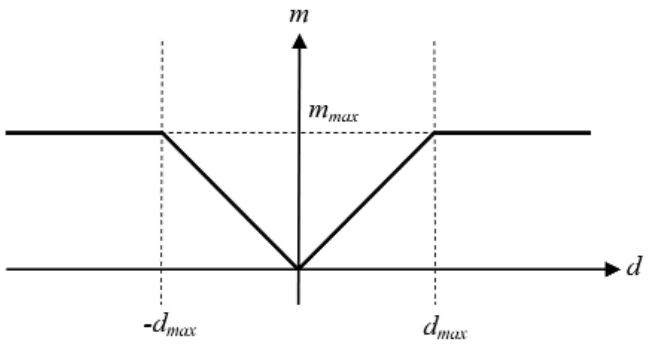

Figure 11. Relation between *m* and *d*.

$$\psi_d = \mathrm{Tan}^{-1}\left(\frac{x_B - x_A}{y_B - y_A}\right) \qquad \ldots (4)$$

$$s = \sqrt{\left(x_B - x_A\right)^2 + \left(y_B - y_A\right)^2}$$

Obviously, the quadrant and signs of the variables need to be handled with care. Nonetheless, the navigation and guidance law given by Equation (4) is actually very basic and crude. It will only direct the aircraft to follow the straight line connecting the moving aircraft and the next target waypoint. This means that if the aircraft encounters significant disturbance such as a strong crosswind, it is very likely that the aircraft will sway away from the original flight path. Hence, it is necessary for the guidance law to guide the aircraft onto the straight line connecting two adjacent waypoints. If this is successfully executed, the aircraft would fly in the desired flight path connected by sequential waypoints. To achieve the goal, a simple straight-line-following guidance law is derived based on Fig. 10. Note that the bearing from the previous waypoint (WP1) to the next waypoint (WP2), σ is always known since the actual co-ordinates of the waypoints are predetermined. Using Equation (4), we may still compute the variables, Ψ_d and *s*. However, instead of asking the aircraft to track Ψ_d, a new line-following heading, Ψ_l is calculated. It is defined by

$$\psi_l = \left(1 - m\right)\sigma + m \cdot \psi_{90}$$

where *m* is a variable that changes depending on the cross-track deviation of the aircraft from the line, *d* (see Fig. 10). A possible relation is illustrated in Fig. 11. It can be clearly seen that when the aircraft is on the line ($d = 0$), *m* becomes zero and the aircraft is to follow the heading, $\Psi_l = \sigma$. Again, the proper values of m_{max} and d_{max} are determined through actual flight testing. Some other relevant equations are given below while the overall structure of the guidance algorithm is shown in Fig. 12. Note that when the distance between the aircraft and waypoint, *s* is less a predetermined threshold, R_{WP}, the aircraft is considered to have reached the target waypoint. Therefore the value R_{WP} is referred to as the waypoint 'pass-through' criterion.

$$\sigma = \mathrm{Tan}^{-1}\left(\frac{x_{WP1} - x_{WP2}}{y_{WP1} - y_{WP2}}\right)$$

$$d = s \cdot \mathrm{Sin}\left(\sigma - \psi_d\right)$$

$$\psi_{90} = \begin{cases} \sigma - 90^\circ, & d \geq 0 \\ \sigma + 90^\circ, & d < 0 \end{cases}$$

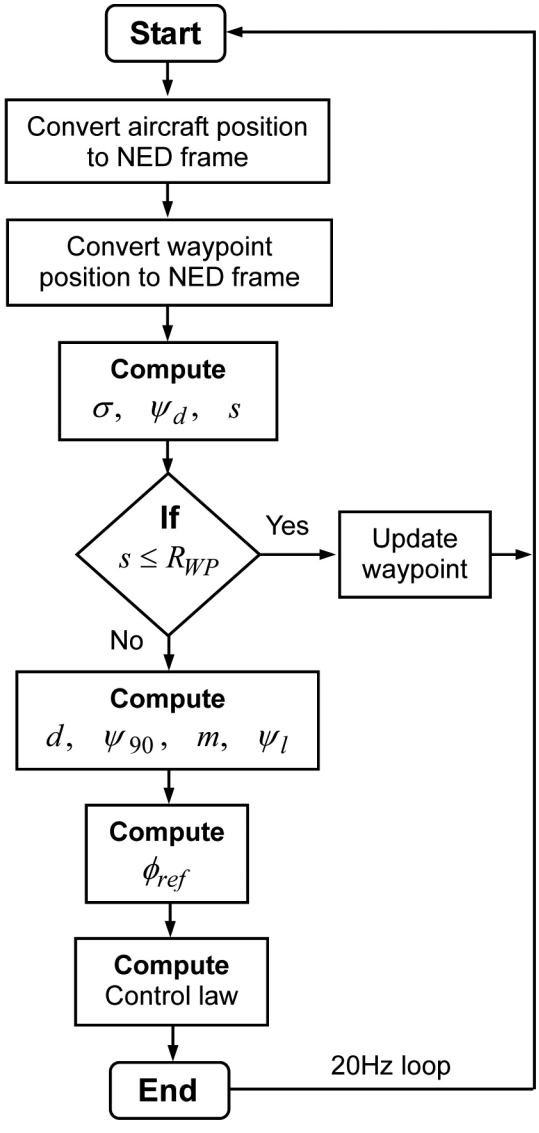

Figure 12. Flowchart of straight-line-following guidance algorithm.

4.0 FLIGHT TEST RESULTS

In order to validate the effectiveness and performance of the automatic flight controllers and the navigation and guidance algorithm described in previous section, a series of flight tests have been conducted using the Spoonbill UAV. Note that all take-offs and landings were performed manually by a ground pilot. Typically, after the aircraft is brought into trimmed, straight and level flight condition at the nominal altitude (ranging from 150m to 300m), the pilot would engage the autopilot. From that point onwards, the aircraft would be fully controlled by the automatic flight control system. The response of the aircraft is observed through visual observation and the wireless data link between the aircraft and the ground control station. The throttle level is kept unchanged throughout all automatic flight modes. However, the pilot has the full authority to disengage the autopilot and regain manual control at anytime if the safety of the aircraft is thought to be compromised. In principle, flight testing of the autopilot was carried out in a gradual,

https://doi.org/10.1017/S0001924000005340 Published online by Cambridge University Press

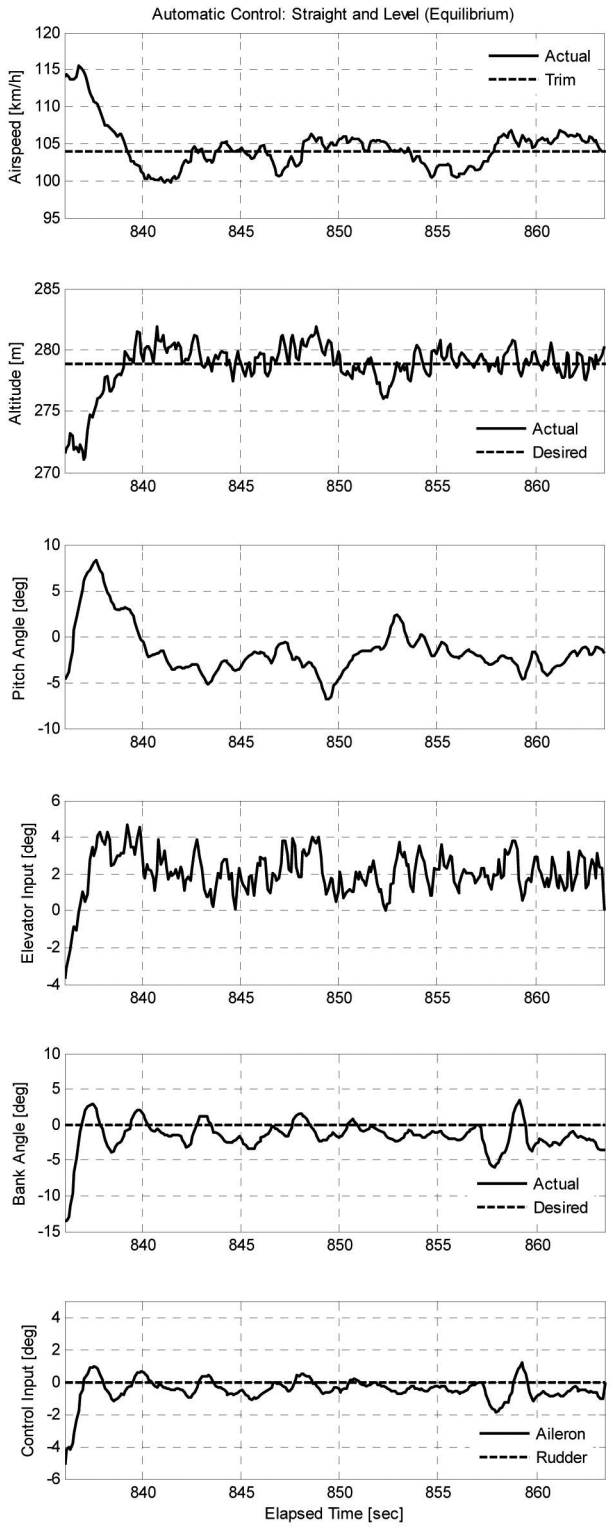

Figure 13. Output responses of straight-and-level (equilibrium) automatic flight.

successive schedule. The inner-loop control (straight-and-level flight) was the first to undergo flight trials. If the baseline LQG controllers fail to maintain the aircraft in its equilibrium condition with sufficient accuracy and resilience over external disturbance, it would be naive to think that all other controllers that build upon that foundation including the heading tracking controller and the navigation and guidance algorithm would perform well at all.

4.1 Straight-and-level (equilibrium) flight

Figure 13 shows a sample of flight data of the aircraft performing successful automatic straight-and-level (equilibrium) flight. For simplicity, the angular rates, i.e. pitch, roll and yaw rates are not plotted. It is evident that the closed-loop control systems for both longitudinal and lateral dynamics are stable. Note that the entire automatic flight lasted for 27·5 seconds and the figure clearly shows that all aircraft outputs settle within a close neighborhood of the desired or trim values throughout the period. The variation of the altitude is bounded between 276m and 282m which means the system error is generally less than 3m (reference altitude is 279m). Moreover, despite having only one control input (elevator deflection) in the longitudinal controller, the airspeed is able to be maintained within an error of 4km/h from the trim airspeed, 104km/h. No distinct oscillation was observed on both airspeed and altitude responses as well. On the other hand, after a short transient process, the bank angle response enters steady state with bounded error generally confined within +5deg. This indicates that the controller is able to maintain the wing at level position under external disturbance (wind gust and aerodynamic load). In addition, the equilibrium condition of the aircraft in flight is being sustained using little control effort. The figure shows that the elevator and aileron typically operate in the order of 4deg and 2deg deflections respectively while the rudder is practically unused. This is one of the strength of linear-quadratic control approach where the compromise between control effectiveness and control effort is accomplished with the proper selection of **Q** and **R** weighting matrices (see Section 3.2).

4.2 Bank angle tracking

In order to evaluate the dynamic tracking performance of the lateral controller on the bank angle response, a square-wave form of desired bank angle trajectory is devised and implemented in test flights. A sample of successful tracking result is shown in Fig. 14. Note that in this particular test run, the desired square wave has an amplitude and period of 20deg and 10sec respectively. As vividly shown in the figure, the bank angle response exhibits excellent transient and steady-state properties. Typically, the overshoot percentage, rise time and settling time lie in the order of 20%, 1·5s and 3s, respectively. Although the 20% overshoot seems to be a bit high, but the absolute magnitude of the overshoot is approximately 4deg which is considered negligible in aircraft practical operations. In addition, the damping of system is more than satisfactory where no noticeable oscillation occurs before the tracking error converges to zero.

4.3 Heading tracking

As mentioned in Section 3.3, if the lateral controller is capable of tracking any arbitrary bank angles with sufficient accuracy, then the aircraft may be controlled to follow a desired heading. First, the simpler design depicted in Fig. 8(a) was put to the test. The initial values of the controller parameters were chosen as: ϕ_{max} = 30deg, Ψ_{th}= 50deg. The corresponding flight test result is featured in Fig. 15(a). In this particular test run, the aircraft initial heading is 278deg (heading West), then it gradually turns towards the North (Ψ = 0deg) responding to the controller's command of a 30deg bank angle. Eventually, the aircraft achieves the desired heading of Ψ = 0deg after approximately 8 seconds. However, note that as the aircraft flies along the North direction, stable but sustained oscillation is observed in the bank angle response. This leads to the slight oscillation in the heading response. The oscillation is caused by the function that relates the heading error and the bank angle command. The bank angle response in Fig. 15(a) shows that there is a phase lag between the actual bank angle and the commanded bank angle when the heading error is getting smaller. This phase lag prevents the aircraft's bank angle from 'catching-up' with the command and thus results in a stable oscillation.

https://doi.org/10.1017/S0001924000005340 Published online by Cambridge University Press

In the attempt to eliminate the oscillation noted previously, a more complex heading controller shown in Fig. 8(b) was designed and tested in flight trial. Note that the parameters needed to fully describe the function are not shown for simplicity. Compared to the former function, more parameters give us more freedom to adjust the gradient of the function in different stages. A well-designed function mitigates the phase-lag phenomenon which in turn eliminates the oscillation. The flight test data in Fig. 15(b) shows that the desired bank angle is tracked with good performance which prevented the oscillation. In addition, the associated aircraft trajectory shown in Fig. 15(b) depicts a smooth turning flight path which features no significant overshoot or oscillation. The result therefore proves that the oscillation occurred in Fig. 15(a) appear to be not related to the yaw-roll coupling instability mode.

On the other hand, albeit being controlled by an independent longitudinal controller, the altitude and airspeed of the aircraft are maintained within close vicinities of their desired values during the entire turning process in both cases. The initial 30deg rolling maneuver causes the altitude to inevitably dip approximately 10-15m. However the controller is able to prevent further altitude drop and recover to the desired altitude after the wing is leveled. Also, although the lateral dynamics is experiencing a sustained oscillation in the case of Fig. 15(a), there seems to be no apparent effect on the longitudinal response. This shows that the decoupled linear models of longitudinal and lateral dynamics is valid and is sufficiently accurate to describe and control the aircraft's motion.

4.4 Waypoint-following automatic flight

As the tests progressing forward, the successful heading tracking test leads to the flight testing of the waypoint-following navigation and guidance law. An anticlockwise square-shape flight route was successfully flown using the basic point-to-point guidance law (see Fig. 16). The circles represent 50m-radius areas around the target waypoints which act as the 'pass-through' criterion. Note, however, that the aircraft merely navigates itself from waypoint to waypoint (WP1 to WP4) without tracing the line connecting them. This means that the aircraft does not follow the desired flight path precisely. The pitfall of this basic navigation rule would be amplified under strong crosswind conditions where the aircraft would deviate considerably away from its flight path. In extreme scenarios where the wind is intolerably large, the aircraft may miss the target waypoints all together.

In conjunction with that, the application of the straight-line-following guidance law yields a noticeable improvement in the flight trajectory as shown in Fig. 17. Note that in both cases, the predetermined waypoint positions are exactly the same. Moreover, both tests were conducted in the same flight sortie so we can safely assume that the wind conditions are similar in order to facilitate legitimate comparison. In short, the figures speak for themselves regarding the effectiveness of the straight-line-following navigation law (Fig. 17) compared with the basic point-to-point guidance law (Fig. 16). Furthermore, recall that d is the perpendicular distance between the aircraft and the flight path as depicted in Fig. 10. The time history of d plotted in both Fig. 16 and Fig. 17 clearly tell the performance of each guidance law. Whenever the aircraft reaches a waypoint and switches to the next one, a surge in d associated with the turning maneuver is observed. However the straight-line-following guidance law would drive d to zero after a short time whereas the value d practically never reaches zero in the case of the basic guidance law.

5.0 CROSS-SEA FLIGHT DEMONSTRATION

The interim conclusion of the Spoonbill project was marked by a cross-sea flight demonstration[7,8]. The mission requires the UAV to make a round-trip automatic flight from Taiwan mainland to a remote island called Dongji, located within the offshore Penghu County which is about 44km away. This mission poses several challenges to the UAV system in terms of reliability of the onboard system, integrity of the airframe structure under sustained engine vibration, susceptibility of the autopilot to significant wind disturbance above sea, accuracy of the navigation and guidance law, *et cetera*. Since full-tank of fuel merely permits one hour of flight, it is vital for the aircraft to follow the desired flight path precisely without significant deviation. After a two-month delay, the milestone event finally took place on 20 October 2009. A total of 18 waypoints were preselected forming a triangular flight path as shown in Fig. 18. A survey on historical weather records of the region reveals that a North wind typically prevails. Therefore, the aircraft was commanded to fly in a clockwise loop so that it will turn "into" the wind at the turning points (WP9 and WP10). This is because turning 'away' from the wind, i.e. turning along the tailwind direction would incur a larger-than-normal turning radius and the risk of losing lift. Indeed, weather record retrieved from the Central Weather Bureau of Taiwan a day later confirmed that an average wind speed of 28·5km/h was sweeping from a bearing of 23deg.

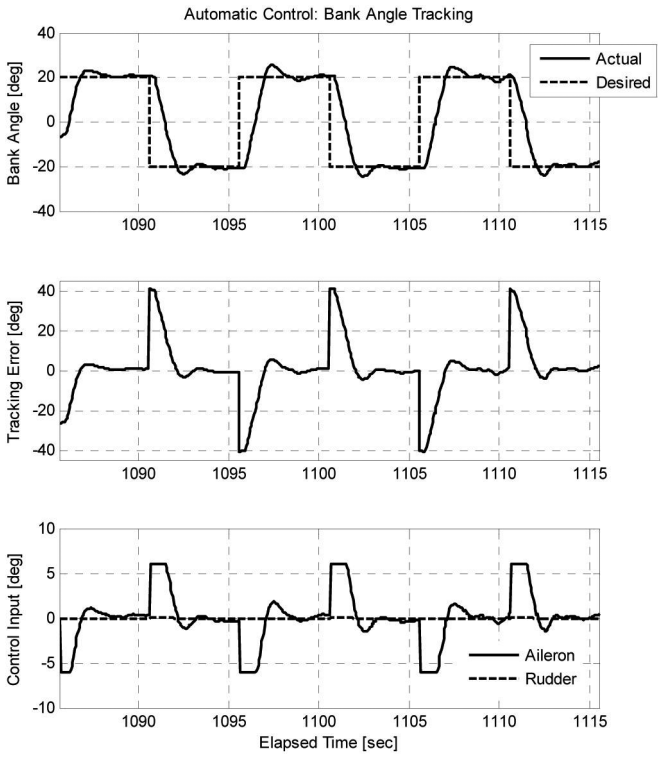

Figure 14. Flight test result of bank angle tracking test.

At 09:17 a.m. local time, SP-80 took off manually from a deserted salt field at Cigu which is located in Southern Taiwan. After climbing to an altitude of approximately 330m, the autopilot was engaged and the aircraft flew straight towards Dongji Island. The aircraft eventually settled at a mean altitude of 331·5m and a mean airspeed of 105km/h. After 4min. 17sec. into the automatic flight mode, the aircraft passed the coastline and flew above the sea for the first time. Figure 19 presents the flight data of the aircraft during the flight leg between waypoint 3 and waypoint 4 (see Fig. 18). Conspicuous oscillations were observed on the aircraft's attitude and air data responses. Albeit not severe and in stable manners, the heading and bank angles oscillate with an amplitude of approximately 7deg and 12deg respectively. This oscillation is caused by the heading controller as described in Section 4.3 since the simpler function depicted in Fig. 8(a) was used in this particular automatic flight. Nonetheless, the motion did not diverge and the aircraft was able to maintain its intended flight path.

https://doi.org/10.1017/S0001924000005340 Published online by Cambridge University Press

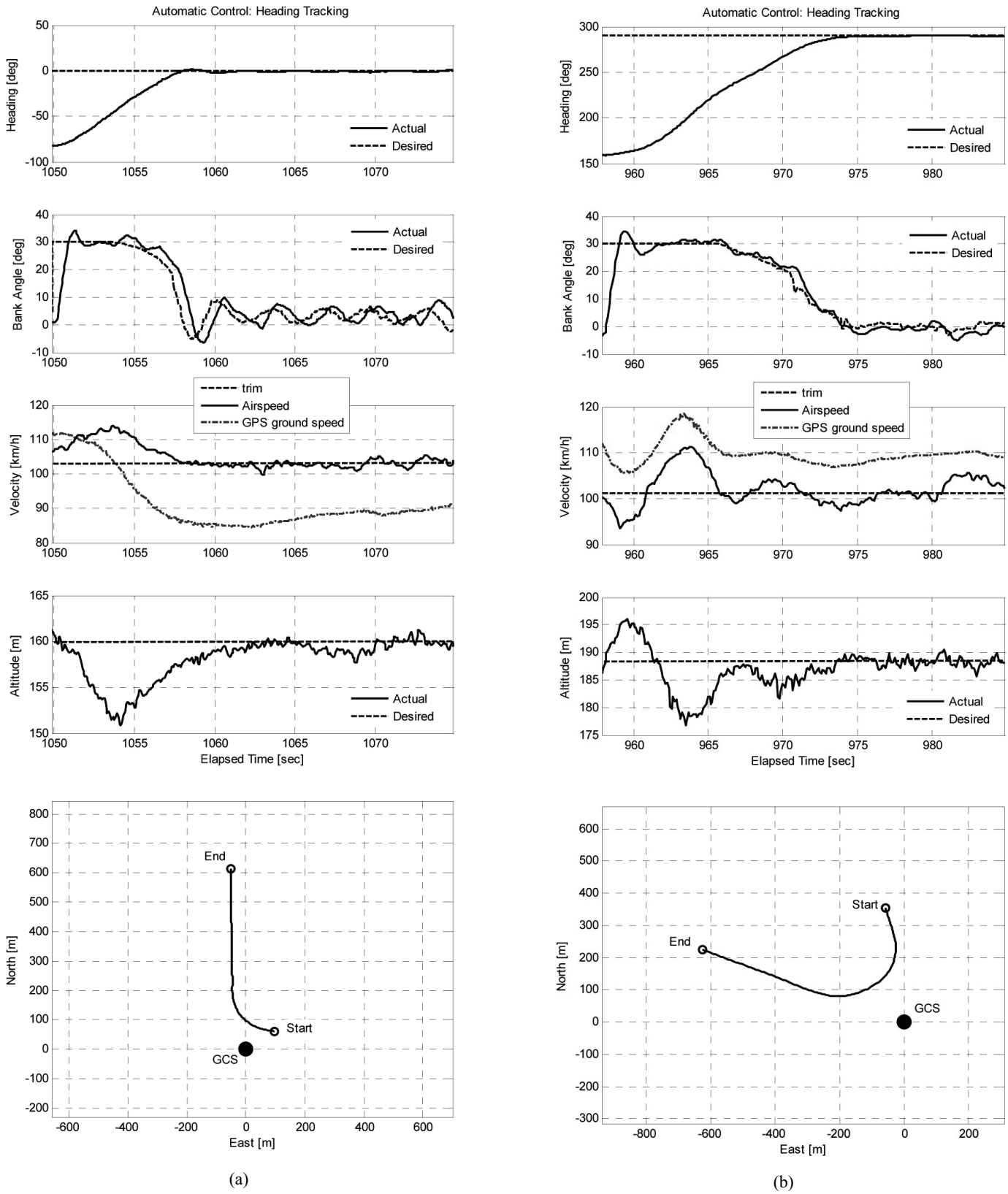

Figure 15. Flight data of heading tracking test: (a) with oscillation; (b) without oscillation..

Interestingly, the longitudinal responses are also found to be oscillating at a period of 6 seconds but with time-varying amplitudes. The same oscillation period of the longitudinal and lateral motions are thought to be coincidental because no further evident of dynamic coupling was found (see Section 4.3). It is noteworthy that at a first glance, it seems that the aircraft is experiencing violent oscillations in altitude. Note, however, that the magnitude of the amplitude is generally less than 5m over a period of 6

https://doi.org/10.1017/S0001924000005340 Published online by Cambridge University Press

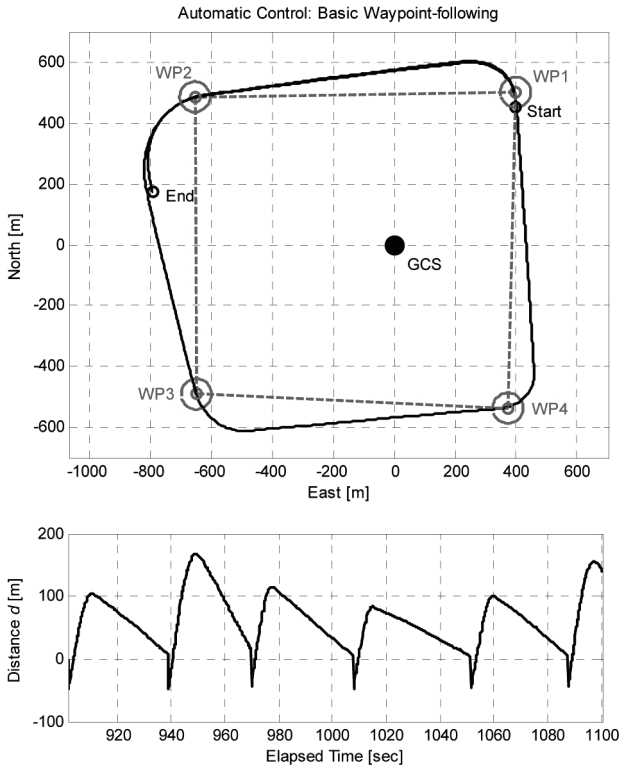

Figure 16. Trajectory of basic waypoint-following automatic flight.

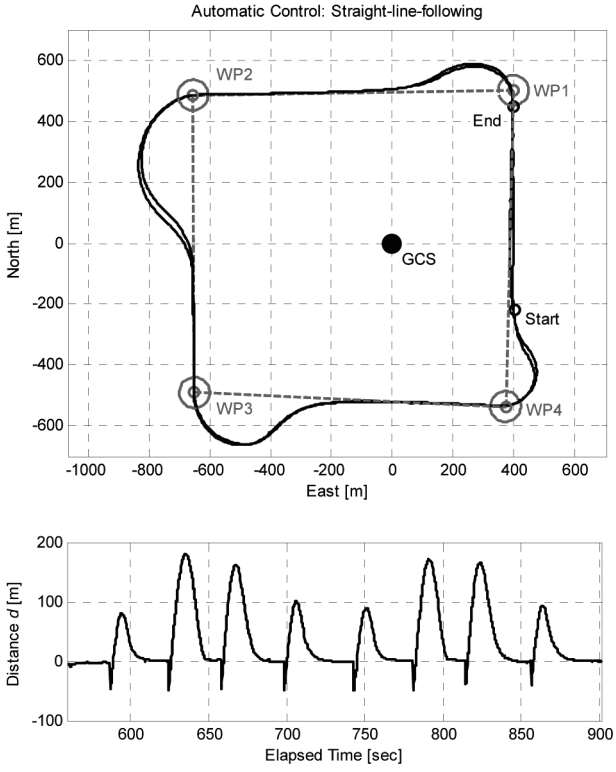

Figure 17. Trajectory of line-following automatic flight.

seconds. Therefore it is more of an illusion due to the compact time scale of the plot. Meanwhile, the oscillations amplitudes are found to be in strong correlation with the fluctuation of engine speed (see Fig. 19, bottom right plot). During the span over 1,140th to 1,220th seconds time mark, the distinct oscillation in the longitudinal responses seems to synchronize with the engine speed's fluctuation. From 1,220th second onwards, the oscillation eases which corresponds well to the engine speed too. To further support this argument, Fig. 20 shows the airspeed versus engine speed plot over the time span of interest. Strong correlation is evident with a calculated correlation coefficient of 0·86. Recall that the autopilot does not control the throttle which in turn dictates the engine speed. The throttle level was kept constant throughout the automatic flight. Variation in the engine speed produces varying thrust which incurs respective variation in the airspeed. When the airspeed fluctuates, the altitude would inevitably fluctuate in the opposite manner due to the exchange between kinetic and potential energy. The longitudinal LQG controller which only has one input (elevator) is unable to cope with such kind of disturbance. It is logical and reasonable to assume that the fluctuation in the engine speed despite a constant throttle setting is initiated by a crosswind of certain strength. This speculation is based on the observation that the oscillation in the engine speed is not sustained over the entire flight. Fortunately, the control system managed to remain stable and maintain safe attitude, airspeed and altitude throughout the entire flight mission despite experiencing relatively strong crosswind.

The strong wind encountered by the aircraft is vividly illustrated in Fig. 21 which shows the airspeed and GPS ground speed measurements when the aircraft was flying in headwind direction between waypoint 9 and 10 (see Fig. 22). A precarious drop in ground speed is observed as soon as the aircraft was aligned with the wind direction. The difference between the airspeed and ground speed gives us an estimate of the incoming wind speed. In particular, a maximum value of 41·42km/h was recorded.

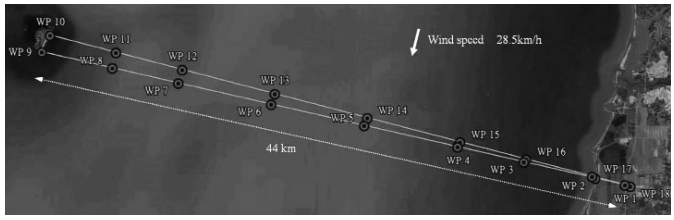

Figure 18. Actual trajectory of the 44km cross-sea automatic flight.

It is interesting to note that the effective range of the wireless data link which relays the aircraft position and flight data back to the ground station is about 25km. Therefore after the aircraft passed waypoint 7 at 09:33 a.m., the data link was totally lost. The signal lost con.dition lasted for about 21 minutes before the data link was resumed at 09:54 a.m. local time. The aircraft was in the returning flight path at the time the data link resumed. Without further incident, the aircraft reappeared in visual sight shortly after it passed the last waypoint. After that, the pilot took over the aircraft and landed it safely at 10:11 a.m. local time. The entire journey took 54min. in the air and the aircraft covered a total ground distance of 90·2km during the automatic flight mode. The solid line in Fig. 18 shows the actual trajectory of the aircraft throughout the entire cross-sea flight while Fig. 22 shows a snapshot of the onboard video image showing the southern shore of Dongji Island.

6.0 CONCLUDING REMARKS

This paper presented a successful design and realization of automatic flight controllers based on the linear-quadratic-Gaussian (LQG) theory on a fixed-wing unmanned air vehicle (UAV). The authors have shown that by using LQG regulators as baseline controllers,

https://doi.org/10.1017/S0001924000005340 Published online by Cambridge University Press

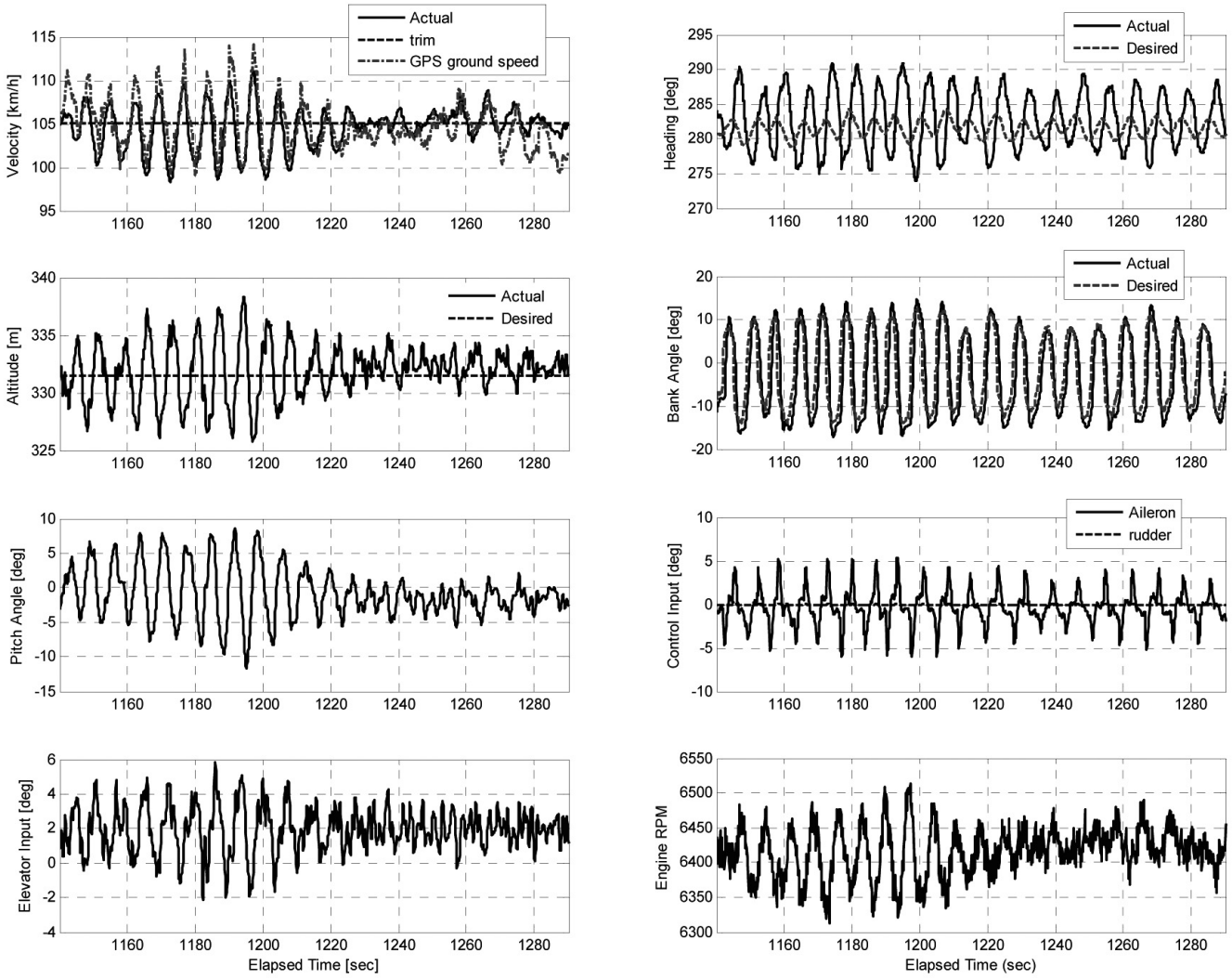

Figure 19. Flight data during flight leg between waypoint 3 and waypoint 4.

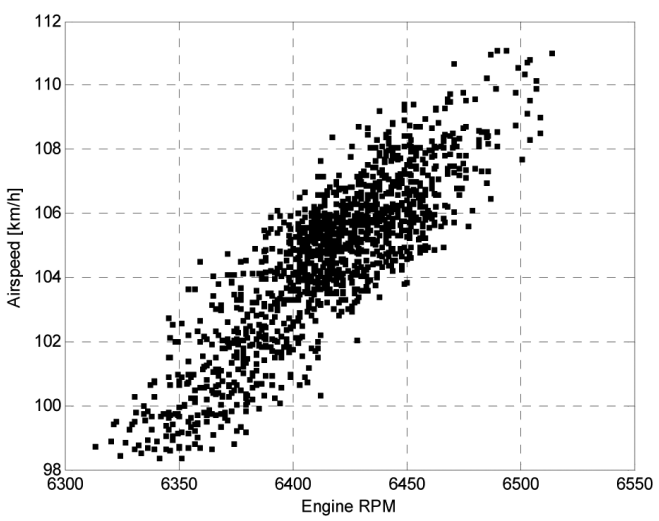

Figure 20. Airspeed versus engine RPM plot with a correlation coefficient of 0·86.

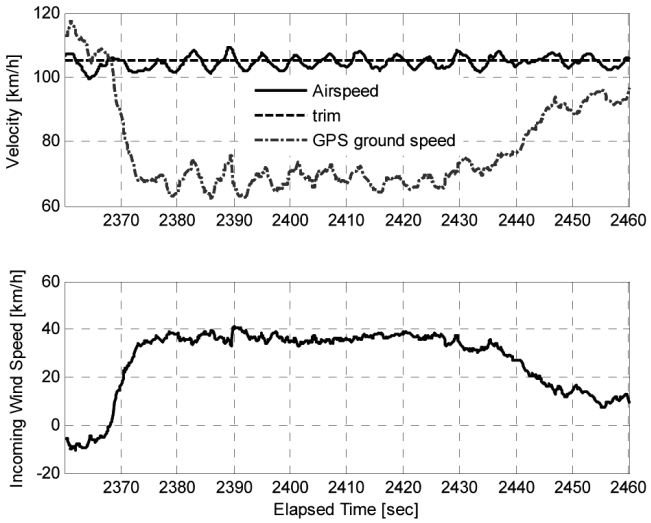

Figure 21. Airspeed and ground speed when the aircraft turned at Dongji Island.

https://doi.org/10.1017/S0001924000005340 Published online by Cambridge University Press

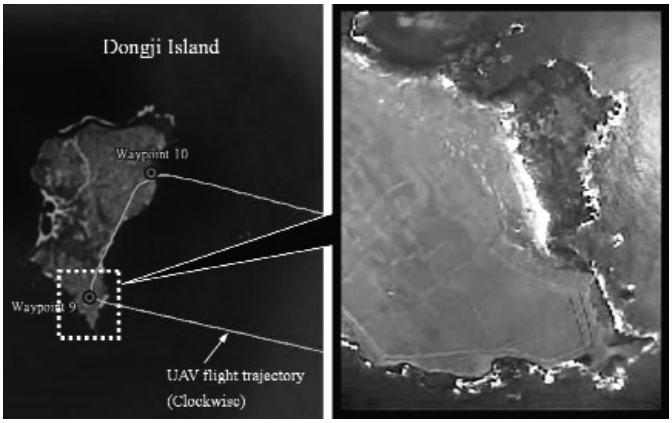

Figure 22. Snapshot of the video image taken by the onboard video camera when Spoonbill UAV was flying over Dongji Island.

automatic flight controllers with nonzero-set-point tracking capability can be built by using simple 'ad hoc' approach. Outer-loop control such as heading tracking and waypoint-following navigation and guidance can thus be accomplished without extensive additional effort once the inner-loop controllers are established. The automatic flight of the Spoonbill UAV is achieved by utilising independent linear longitudinal and lateral controllers which are separately designed. Flight test results have shown that the controllers perform very well even though simplified linear models are used in the synthesis of the controllers. In addition, the controllers exhibit exceptional stability and tracking performance with good disturbance rejection capability. No evidence of significant cross-coupling dynamics between longitudinal and lateral motions was found. Also, the resulting control laws are simple and efficient enough to be easily realized using limited onboard computing power.

The flight controllers proposed in this paper, however, are not without limitations. First, the decoupled linear models and independent controllers for longitudinal and lateral dynamics are only valid for the conventional fixed-wing (tail-aft) type of UAV. Any other configurations would require modification in the model structure. Note, however, that as long as the dynamic model is casted in linear, proper state-space representation, the LQG control synthesis outlined in this paper is still applicable. Next, it should be noted that actuator dynamics are not incorporated into the design of the closed-loop control system. This means that the response time between control input and surface deflection is assumed to be negligible. This assumption is valid largely because of the relatively small gross weight of the Spoonbill UAV. At 30kg of gross weight, the aerodynamic loads acting on the control surfaces would be small enough to permit the use of electric servomotors as the actuators. High-performance servomotors generally have a lag time that is essentially negligible. Most importantly, extensive flight-test results did not seem to uncover degraded performance linked to the time delay effect associated with the actuator dynamics. Nevertheless, as the above discussion suggests, the same assumption may not be applicable to large UAVs, especially those which use elaborate electro-mechanical or hydraulic actuator system.

With all that being said, the best testament of the effectiveness and practicality of the proposed flight controllers is the successful cross-sea flight demonstration which took place on 20 October 2009. The 54min. over-sea flight stretched the performance, reliability, and robustness of the entire flight control system of the Spoonbill UAV to its limit. Nevertheless, though successful, the milestone flight shed crucial light on the performance and behaviour of the close-loop control system under sustained, severe external disturbance, i.e. harsh atmospheric condition over sea. In particular, the engine speed experienced noticeable fluctuation despite the throttle being kept constant. It is thought to be the primary reason of the corresponding oscillation in the longitudinal responses. In future, throttle input may be included into the longitudinal model which should further improve the stability and controllability of the airspeed response. In short, the stability and robustness issues of the LQG controller require further analysis and investigations before it can be extended to the automatic control of other phases of flight such as climbing and descending, circular loitering, three-dimensional path following, et cetera. In addition, better navigation and guidance algorithm with more rigorous theoretical background is also another area of work that is identified for future attention.

ACKNOWLEDGEMENT

This work is supported by the National Cheng Kung University, Taiwan, ROC under grant number, D98-3340 and D99-3340, under the Ministry of Education's 5Y50B Special Funding.

REFERENCES

1. ERDOS, D. and WATKINS, S.E. UAV Autopilot integration and testing, 2008, IEEE Region 5 Conference, pp 1-6.
2. BEARD, R., KINGSTON, D., QUIGLEY, M., SNYDER, D., CHRISTIANSEN, R., JOHNSON, W., MCLAIN, T. and GOODRICH, M.A. Autonomous vehicle technologies for small fixed-wing UAVs, *J Aerospace Computing, Information, and Communication*, January 2005, **2**, pp 92–108.
3. HSIAO, F.B., HSIEH, S.Y., CHAN, W.L. and LAI, Y.C. Engine speed and velocity controller development for small unmanned aerial vehicle, *J Aircr*, 2008, **45**, (2), pp 55-65.
4. MONTGOMERY, P.Y. Carrier Differential GPS as a Sensor for Automatic Control, 1996, PhD thesis, Stanford University.
5. CHO, A., KIM, J., LEE, S., CHOI, S., LEE, B. and KIM, B. Fully automatic taxiing, takeoff and landing of a UAV only with a single-antenna GPS receiver, 2007, Proceedings of AIAA Infotech@Aerospace 2007 Conference and Exhibit, Rohnert Park, California, USA..
6. TUZCU, I., MARZOCCA, P., CESTINO, E., ROMEO, G. and FRULLA, G. Stability and control of a high-altitude, long-endurance UAV, *J Guidance, Control and Dynamics*, May-June 2007, **30**, (3), pp 713-721.
7. LEE, C.S., HSIAO, F.B. and JAN, S.S. Design and implementation of linear-quadratic-Gaussian stability augmentation autopilot for unmanned air vehicle, *Aeronaut J*, May 2009, **113**, (1143), pp 275-290.
8. LEE, C.S., CHAN, W.L. and HSIAO, F.B. The Development of Spoonbill UAV and LPV modeling of longitudinal dynamics, 2008, Proceedings of 23rd Bristol International UAV Systems Conference, April 2008, Bristol, UK.
9. LEE, C.S., CHAN, W.L. and HSIAO, F.B. Implementation of system identification on unmanned aerial vehicle via subspace and prediction error method, *J Aeronautics, Astronautics and Aviation*, 2010, Series A, **42**, (2), pp 87-98.
10. LEE, C.S. The Realization of Optimal Stability Augmentation Autopilot for Unmanned Air Vehicle, 2008, Master thesis, Institute of Aeronautics and Astronautics, National Cheng Kung University, Taiwan.
11. NELSON, R.C. *Flight Stability and Automatic Control*, 1998, Second edition, (Chapter 4-5), WCB/McGraw-Hill.
12. OGATA, K. *Discrete-Time Control Systems*, 1987, Prentice-Hall.
13. STEVENS, B.L. and LEWIS, F.L. *Aircraft Control and Simulation*, 2003, Second edition, John Wiley & Sons.

https://doi.org/10.1017/S0001924000005340 Published online by Cambridge University Press